Computer Three-Dimensional Reconstruction of the Atrioventricular Node
ONLINE DATA SUPPLEMENT

J. Li; I.D. Greener; S. Inada; V.P. Nikolski; M. Yamamoto; J.C. Hancox, H. Zhang, R. Billeter; I.R. Efimov; M.R. Boyett; H. Dobrzynski

Methods

Animals. ~2 kg New Zealand White rabbits (provided by Washington University, St. Louis, USA or University of Leeds, UK) were sacrificed in accordance with the guidelines of the American Heart Association or according to the United Kingdom Animals (Scientific Procedures) Act, 1986.

Electrophysiology. The AVN preparation used to construct the model was first electrophysiologically mapped using fluorescent imaging. In brief, the preparation was stained with di-4-ANEPPS (1 μM in perfusate) and voltage-sensitive fluorescent signals were recorded from a 8×8 mm area of the AVN at a rate of 1500 frames/s using a 16×16 photodiode array as previously described.[1] The excitation-contraction uncoupler, 2,3-butanedione monoxime (15 mM), was added to the perfusate to suppress motion artefacts. Signals were low-pass filtered at 120 Hz, differentiated, normalised by the basic beat recordings, and plotted as two-dimensional intensity graphs, which were overlapped as frames with the image of the preparation to produce animations. Wavefronts of activation were visualised in these animations in order to identify the anatomical location of the pacemaker and conduction pathways.[1] The preparation was digitally photographed and the field of view was identified with an accuracy of 0.2 mm.

Paraffin-embedding and sectioning. Following electrophysiology, the preparation was paraffin-embedded: in brief, the preparation was fixed in 10 % neutral buffered formalin for 24 h, washed in 70 % ethanol for 2 h and embedded in paraffin overnight. The paraffin-embedded preparation was sectioned: ~10 μm sections were cut and mounted on Superfrost Plus glass slides (BDH, Leicester, UK).

Histology. Paraffin-embedded sections at each of 65 levels were de-waxed in Histoclear (Fisher Scientific, Loughborough, UK), hydrated through graded ethanols (100 to 70 %), post-fixed in Bouin's fluid for 15 min, and washed three times in 70 % ethanol (each wash 10 min). The sections were stained with Masson's trichrome as previously described.[2] After staining, sections were dehydrated through graded ethanols (70 to 100 %), cleared in Histoclear and mounted in DPX mounting medium (BDH) for permanent mounting. With the Masson's trichrome technique, nuclei are stained dark blue/black, myocytes are stained purple and connective tissue is stained blue. Masson's trichrome stained sections were stored at room temperature for subsequent viewing with a Leica Materials Workstation (Leica Microsystems, Wetzlar, Germany) or a Zeiss Axio Imager.Z1 microscope fitted with an AxioCam HRc camera and Axiovision software (Carl Zeiss, Germany). High definition images of the sections were collected by making a mosaic of images collected with a 10× objective.

Antibodies. Antibodies used were: (a) mouse monoclonal antibody to middle (160/165 kD) neurofilament - either MAB5254 (Chemicon, Harrow, UK) or 2H3 (Developmental Studies Hybridoma Bank, University of Iowa, USA); (b) mouse monoclonal antibody to connexin43 (Cx43) (MAB3068; Chemicon).

Immunoenzyme labelling. Prior to the immunoenzyme technique, sections from each of the 65 levels were dewaxed in xylene and treated with 100 % ethanol for 10 min. The sections were then treated with H_2O_2 in methanol (2 ml of 30 % solution of H_2O_2 per 100 ml of methanol) for 30 min. Sections were treated with an antigen unmasking solution (H-3300; Vector Labs, Peterborough, UK) according to the manufacturer's instructions in a microwave for 10 min at boiling point. Sections were treated with 0.2 % Triton-X 100 diluted in phosphate buffered saline (PBS) for 30 min, washed in PBS three times (each wash 10 min) and blocked in normal horse serum (diluted in PBS according to the instructions in the Vectastain ABC kit, PK-6102, Vector Labs) for 60 min. Sections were labelled with the anti-neurofilament and anti-Cx43 primary antibodies for 24 h at 4°C. Each primary antibody was diluted in 1 % bovine serum albumin in PBS and used at a dilution of 1:100. After incubation in the primary antibodies, the sections were washed three times in PBS over 30 min, and incubated with biotinylated anti-mouse secondary antibody for ~2 h and washed again three times in PBS over 30 min. Sections were incubated in ABC reagents for 60 min and this was again followed by three washes in PBS over 30 min. The biotinylated anti-mouse secondary antibody and ABC reagents were prepared according to the instructions in the Vectastain ABC kit. Sections were developed in DAB solution for 5-10 min. DAB solution was prepared according to the instructions in the Vector Peroxidase Substrate Kit (SK-4100; Vector Labs). Finally, sections were washed in distilled H_2O for 10 min, dehydrated in graded ethanols (50 to 100 %), cleared in xylene, and mounted in a permanent mounting medium (VectaMount; H-5000; Vector Labs). No labelling above background was obtained when the primary antibodies were omitted (data not shown). Immunoenzyme labelled sections were stored at room

temperature for subsequent viewing with the Leica or Zeiss systems. High definition images of the sections were collected by making a mosaic of images collected with a 10× objective.

Measurement of myocyte orientation. The Masson's trichrome stained sections were inspected under the microscope with a 40× or 63× objective. The approximate myocyte orientation was determined manually: myocytes with a round shape were assumed to be running perpendicular to the plane of the section (e.g. Fig. S1A); myocytes with a long elliptical shape were assumed to be running in the plane of the section (e.g. Fig. S1B).

Three-dimensional (3D) reconstruction of the AVN. Corel Draw (version 11.0; Corel Corporation, Ontario, Canada) and MATLAB (version 6.5; The MathWorks, Inc., Matick, MA, USA) were used to analyse the images and construct a 3D anatomical model of the AVN. There were six steps in this process. **Step 1. Segmentation.** In the Masson's trichrome stained sections, various tissue types could be identified: myocytes were stained purple, connective tissue was stained blue and fatty tissue was white. On the images of the Masson's trichrome stained sections, Corel Draw was used to outline the various tissue types (carried out manually) and highlight them with a colour unique to that cell type. The result was two-dimensional "model sections" showing the distribution of myocytes and connective and fatty tissue. **Step 2. Further segmentation.** The Masson's trichrome stained sections were compared with adjacent neurofilament and Cx43 labelled sections to distinguish different myocyte types: (i) neurofilament-positive, loosely-packed, Cx43-negative nodal tissue, (ii) neurofilament-positive, densely-packed, Cx43-positive nodal tissue, (iii) neurofilament-positive, loosely-packed, Cx43-positive nodal tissue, (iv) neurofilament-negative, loosely-packed, Cx43-positive transitional tissue, (v) neurofilament-negative, densely-packed, Cx43-positive atrial muscle and (vi) neurofilament-negative, densely-packed, Cx43-positive ventricular muscle. This information was incorporated into the model sections. **Step 3. Correction.** When the shape of a section was unchanged, but the section was affected by some combination of translation, rotation and scaling, linear conformal transformation was used. Let the x axis be from right to left, the y axis be from ventral to dorsal, the z axis be from caudal to cranial and

$$sc = scale * \cos(angle)$$

and

$$ss = scale * \sin(angle).$$

Then

$$[u \quad v] = [x \quad y \quad 1] * \begin{bmatrix} sc & -ss \\ ss & sc \\ tx & ty \end{bmatrix}, \qquad (1)$$

where *x* and *y* are the coordinates of the input section we want to transform and *u* and *v* are the coordinates of the output section. Equation 1 was solved for *sc*, *ss*, *tx* and *ty*. At least two control-point pairs are needed to solve for the four unknown coefficients. **Step 4. Alignment.** Alignment of the model sections was crucial to model development. The tract of nodal tissue, tendon of Todaro, coronary sinus, and the bottom edge of the preparation were the main landmarks used to align the sections as will be explained. Fig. S2 shows three screenshots from the custom written programme used for correction and alignment. The current model section being worked on is shown in colour in the bottom half of the screen; the previous section is shown in greyscale in the top half of the screen. In Fig. S2A, in the top half of the screen, the outline of the *current* section is shown in red. This demonstrates that the correspondence between the current section and the previous section is good. In Fig. S2B, in the top half of the screen, the outline of the tendon of Todaro in the current section is shown in red; again the correspondence between the tendon of Todaro in the current and previous sections is good. In Fig. S2C, in the top half of the screen, the outline of the compact node in the current section is shown in red; again the correspondence between the compact node in the current and previous sections is good. After all the sections had been aligned in this way, the envelope of the model sections was superimposed on a photograph of the original preparation (Fig. S3). Note that the starting and end points of the sectioning (in relation to the original preparation) were known. The bottom edge of the original envelope of model sections is shown by the dotted line (*f(z), nonlinear function*) in Fig. S3 and it does not correspond exactly to the bottom edge of the original preparation (solid line: *g(z), nonlinear function*). The alignment of the sections was next corrected: let

ty(z) = g(z) – f(z);

then

$v(z) = y(z) + ty(z)$.

Step 5. Regularising the array. The original sections were at variable interval. Piecewise linear interpolation was used to interpolate model sections to obtain model sections at a regular 50 μm interval; this increased the number of model sections from 65 to 174. **Step 6. Visualising the model.** The isosurface method was used to view the model. The 3D array model (File 1) is available as part of the Online Data Supplement.

Cellular automaton model. We simulated the spread of activation using the cellular automaton model.[3] The cellular automaton model, although simple, is a useful model to calculate the activation sequence in the heart.[4,5] The anatomical model consists of ~13 million 'nodes'. Each node is equivalent to a cluster of myocytes or connective tissue. According to the cellular automaton model, each of the ~13 million nodes in the anatomical model at time, t, is assigned a state, $u_i(t)$, where the subscript refers to the node number (Fig. S4A). Each node can be in one of three states: resting, excited or refractory. If $u_i(t) = 0$, myocyte node *i* is in its resting state and can be excited by neighbouring myocyte nodes. However, as expected, myocyte node *i* cannot excite neighbouring myocyte nodes. The definition of neighbouring nodes to node *i* is shown in Fig. S4B. If node *j* is in an ellipsoid centred on node *i*, node *j* is defined as a neighbouring node of node *i* (Fig. S4B). However, if there are connective tissue nodes between node *i* and *j*, node *j* is not defined as a neighbouring node of node *i*. The use of an ellipsoid (Fig. S4B) allows for the anisotropic properties of cardiac tissue. We assumed an anisotropic ratio of the radii in the longitudinal direction (parallel to the long axis of myocytes) and the two transverse directions (perpendicular to the long axis) – i.e. R_L:R_T - of 3:1 (Table S1). In the anatomical model, myocyte orientation was assumed to vary throughout the AVN conduction axis as shown in Fig. S4C (a simplified version of myocyte orientation based on Fig. 6).

The conduction velocity varies throughout the atrioventricular junction: the conduction velocity of the atrial muscle of the triangle of Koch in the rabbit is 35±17 cm/s[1], whereas the conduction velocity of the 'N region' (possibly the inferior nodal extension) in the rabbit is 2-10 cm/s.[6] In large part, this is likely to be the result of changes in electrical coupling in different regions of the AV junction. Pollack[7] reported that, in the rabbit, coupling (assessed by dye transfer between cells) between AVN myocytes was at least three orders of magnitude lower than between atrial myocytes. Electrical coupling is provided by connexins. Connexin43 (Cx43) forms 60–100 pS gap junction channels and is abundant in the atrial muscle of the rabbit.[e.g.8] In contrast, Cx43 mRNA and protein are largely absent from the inferior nodal extension of the rabbit.[8,9] Instead, connexin45 (Cx45), which forms 20–40 pS gap junction channels, is expressed in the inferior nodal extension of the rabbit.[8] Electrical coupling is likely to be stronger in the penetrating bundle of the rabbit, because some Cx43 (mRNA and protein) is expressed in this region.[8,9] R_L and R_T were varied between tissues (Table S1) to vary the electrical coupling. It was assumed that the electrical coupling of atrial muscle=transitional zone>penetrating bundle>inferior nodal extension. R_L and R_T were varied manually to obtain conduction velocities consistent with those measured in experiments.

If $\frac{P_i}{E_i + P_i} < u_i(t) \le 1$, myocyte node *i* is in its excited state (where E_i and P_i are the excited period and the refractory period, respectively). E_i was assumed to be 5 ms. If myocyte node *i* is in its excited state, node *i* is able to excite neighbouring myocyte nodes. If $0 < u_i(t) \le \frac{P_i}{E_i + P_i}$, myocyte node *i* is in its refractory state and can neither be excited by neighbouring myocyte nodes or excite neighbouring myocyte nodes. For resting myocyte node *i* to switch into the excited state, two requirements must be met: $u_i(t) = 0$, i.e. myocyte node *i* must be in the resting state; and $\sum_j e_j > \theta_i$, i.e. the sum of the excitatory electrotonic current from neighbouring cells must be greater than a critical threshold, θ_i (assumed to be 1). The refractory period, P_i, is known to vary among the tissues of the AVN conduction axis: atrial muscle<slow pathway<fast pathway (Table S2). This was incorporated into the model (Table S3; Fig. S4D).

Monodomain model. We also simulated the spread of activation using the monodomain model. With the monodomain model, biophysically-detailed models of the action potential were used. For atrial muscle, the Lindblad et al.[10] model of the rabbit atrial action potential was used. For the rabbit AVN, based on experimental data, we have recently developed a family of action potential models.[11] At the rabbit AVN, three types of myocyte have been identified: true nodal N-type myocytes, transitional AN-type myocytes

(with properties between those of the N myocytes and the atrial myocytes) and transitional NH myocytes (with properties between those of the N myocytes and the myocytes of the bundle of His).[12] For example, atrial myocytes possess Na^+ current (I_{Na}) and lack the pacemaker current (I_f) and consequently have a fast action potential and do not exhibit pacemaking. In contrast, AVN myocytes with N-type action potentials generally lack I_{Na} and possess I_f, and consequently they have a slow action potential and many of them exhibit pacemaking.[13] Distinct electrophysiological features of myocytes with AN- and NH-type action potentials have also been reported.[13] We developed models for all three myocyte types.[11] We assumed AN myocytes make up the transitional zone, N myocytes make up the inferior nodal extension and NH myocytes make up the penetrating bundle. This is consistent with ion channel expression in these three regions: the inferior nodal extension has the most nodal type ion channel expression profile (e.g. it lacks $Na_v1.5$, responsible for I_{Na}, and it expresses HCN4, responsible for I_f), whereas the transitional zone and penetrating bundle have a more transitional ion channel expression profile (e.g. it is likely that they express some $Na_v1.5$ and less HCN4).[9]

Within the inferior nodal extension, g_{Na} was assumed to change in a sigmoidal fashion:

$$g_{\mathrm{Na}} = \frac{0.5\times10^{-12}}{1.0+\exp\left(\frac{x-5.6}{-5.0}\right)}, \tag{2}$$

where x is the distance (in mm) from the left side of the anatomical model.

The excitable behaviour of cardiac tissue was modelled as a continuous system using the following partial differential equation, usually referred to as the monodomain model:

$$\frac{\partial V}{\partial t} = -\frac{1}{C_{\mathrm{m}}}\left(I_{\mathrm{ion}} + I_{\mathrm{stim}}\right) + \left(D_x\frac{\partial^2 V}{\partial x^2} + D_y\frac{\partial^2 V}{\partial y^2} + D_z\frac{\partial^2 V}{\partial z^2}\right), \tag{3}$$

where C_m is the membrane capacitance, I_{ion} is the sum of ionic currents, D_x, D_y and D_z are diffusion coefficients in the x, y and z planes, and I_{stim} is stimulus current. I_{stim} was a current pulse 10 nA in amplitude and 1 ms in duration and it was injected into the atrial muscle of the crista terminalis. The diffusion coefficients are a measure of electrical coupling. We assumed an anisotropic ratio of the diffusion coefficients in the longitudinal direction (parallel to the long axis of myocytes) and the two transverse directions (perpendicular to the long axis) – i.e. D_L:D_T - of 3:1 (Table S1) – compare to the use of the cellular automaton model. Once again, in the anatomical model, myocyte orientation was assumed to vary throughout the atrioventricular conduction axis as shown in Fig. S4C (a simplified version of myocyte orientation based on Fig. 6). D_L and D_T were varied between tissues (Table S1) to vary the electrical coupling. It was assumed that the electrical coupling of atrial muscle>transitional zone=inferior nodal extension=penetrating bundle. D_L and D_T were varied manually (not iteratively; c.f.[14]) to obtain conduction velocities consistent with those measured in experiments.

All simulations were coded in C++ and MPI (message passing interface) and were run on 40 nodes of a computer cluster with the Linux operating system. A Runge-Kutta numerical integration method (RKF45) was used to solve the ordinary differential equations. The time step was 5 μs, which gave a stable solution of the equations and maintained the accuracy of the computation of membrane current and potential. The voxel size of the anatomical model was reduced to 100×100×100 μm to make the model tractable (100 μm is close to the length of myocytes).

Measurement of local conduction velocity. An algorithm was used to determine the local conduction velocity vector. Let the spatial coordinates of a node be x, y and z and its activation time be $t_{x,y,z}$. At the node, the conduction velocities in the three planes (v_x, v_y and v_z) were calculated by dividing the distance from the previous node to the next node by the activation time delay between the two nodes:

$$v_x = \frac{2\Delta x}{t_{x+1,y,z} - t_{x-1,y,z}}, v_y = \frac{2\Delta y}{t_{x,y+1,z} - t_{x,y-1,z}}, v_z = \frac{2\Delta z}{t_{x,y,z+1} - t_{x,y,z-1}}, \tag{4}$$

where Δx, Δy and Δz are the distances (100 μm) between two nodes in the three planes. The conduction velocity at (x, y, z), $\mathbf{v}_{x,y,z}$, is defined as follows,

$$\mathbf{v}_{x,y,z} = v_x\mathbf{i} + v_y\mathbf{j} + v_z\mathbf{k}, \quad (5)$$

where **i**, **j** and **k** are unitary vectors in the x, y and z directions, respectively. The magnitude of the conduction velocity, $|\mathbf{v}_{x,y,z}|$, is defined as follows,

$$\left|\mathbf{v}_{x,y,z}\right| = \sqrt{v_x^{\,2} + v_y^{\,2} + v_z^{\,2}}\,. \quad (6)$$

Limitations of the study

In the present study, myocyte orientation was only measured approximately and in the future it should be measured accurately with a technique such as diffusion tensor MRI.[15] The structure-function relationships of the anatomical model need to continually refined as we discover more about the expression of gap junctions and ion channels in the AVN,[9] nervous innervation of the AVN, and remodelling of the AVN in disease. Although the behaviour of the AVN in isolation is important, the behaviour of the AVN should also be understood in the context of the whole heart – currently, we are developing an anatomical model of the right atrium including the SAN and AVN.[16]

Sources of Funding

This work was supported by the British Heart Foundation (programme grant, RG/06/005) and the Biotechnology and Biological Sciences Research Council (e-science grant, BBS/B/1678X).

References

1. Nikolski VP, Jones SA, Lancaster MK, Boyett MR, Efimov IR. Cx43 and dual-pathway electrophysiology of the atrioventricular node and atrioventricular nodal reentry. *Circ Res.* 2003;92:469-475.
2. *Theory and Practice of Histological Techniques*. Harcourt Publishers Ltd.; 2002.
3. Bub G, Tateno K, Shrier A, Glass L. Spontaneous initiation and termination of complex rhythms in cardiac cell culture. *J Cardiovasc Electrophysiol.* 2003;14:S229-S236.
4. Greenberg JM, Hauer RN. Spatial patterns for discrete models of diffution in excitable media. *SIAM J Appl Math.* 1978;34:515-523.
5. Gerhardt M, Schuster H, Tyson JJ. A cellular automation model of excitable media including curvature and dispersion. *Science.* 1990;247:1563-1566.
6. Efimov IR, Nikolski VP, Rothenberg F, Greener ID, Li J, Dobrzynski H, Boyett M. Structure-function relationship in the AV junction. *Anatom Rec.* 2004;280A:952-965.
7. Pollack GH. Intercellular coupling in the atrioventricular node and other tissues of the rabbit heart. *J Physiol.* 1976;255:275-298.
8. Dobrzynski H, Nikolski VP, Sambelashvili AT, Greener ID, Boyett MR, Efimov IR. Site of origin and molecular substrate of atrioventricular junctional rhythm in the rabbit heart. *Circ Res.* 2003;93:1102-1110.
9. Greener ID, Tellez JO, Dobrzynski H, Yamamoto M, Billeter-Clark R, Boyett MR. Distribution of ion channel transcripts in the rabbit atrioventricular node as studied using in situ hybridisation and quantitative PCR. *J Mol Cell Cardiol.* 2006;40:982-983.
10. Lindblad DS, Murphey CR, Clark JW, Giles WR. A model of the action potential and underlying membrane currents in a rabbit atrial cell. *Am J Physiol.* 1998;271:H1666-H1696.
11. Inada S, Hancox JC, Zhang H, Boyett MR. Mathematical model of the atrioventricular node. *Proceedings of the Physiological Society.* 2007;PC29.
12. deCarvalho AP, de Almeida DF. Spread of activity through the atrioventricular node. *Circ Res.* 1960;8:801-809.
13. Munk AA, Adjemian RA, Zhao J, Ogbaghebriel A, Shrier A. Electrophysiological properties of morphologically distinct cells isolated from the rabbit atrioventricular node. *J Physiol.* 1996;493:801-818.
14. Chinchapatnam PP, Rhode KS, King A, Gao G, Ma Y, Schaeffter T, Hawkes D, Razavi RS, Hill DL, Arridge S, Sermesant M. Anisotropic wave propagation and apparent conductivity estimation in a fast electrophysiological model: application to XMR interventional imaging. *Med Image Comput Comput Assist Interv Int Conf Med Image Comput Comput Assist Interv.* 2007;10:575-583.

15. Aslanidi OV, Buckley DL, Boyett MR, Zhang H, Molenaar P, Dobrzynski H. Diffusion tensor magnetic resonace imaging of the human sinoatrial and atrioventricular nodes. *Heart Rhythm.* 2007;4:S160.
16. Li J, Schneider JE, Yamamoto M, Greener ID, Dobrzynski H, Boyett MR. A detailed 3D model of the rabbit right atrium including the sinoatrial node, and atrioventricular node, surrounding blood vessels and valves. *Computers in Cardiology.* 2005;32:25-28.
17. Reid MC, Billette J, Khalife K, Tadros R. Role of compact node and posterior extension in direction-dependent changes in atrioventricular nodal function in rabbit. *J Cardiovasc Electrophysiol.* 2003;14:1342-1350.
18. Lin LJ, Billette J, Medkour D, Reid MC, Tremblay M, Khalife K. Properties and substrate of slow pathway exposed with a compact node targeted fast pathway ablation in rabbit atrioventricular node. *J Cardiovasc Electrophysiol.* 2001;12:479-486.

Movies and File

Movie 1. Animation of the 3D anatomical model of the AVN. See Fig. 5 for a key to the colours. During the course of the movie, different cell types are removed to reveal underlying structures.

Movie 2. Simulation of anterograde conduction through the AVN using the monodomain model. The preparation was stimulated at the interatrial septum as shown by the stimulating electrodes. There is a flash and click coincident with the stimulus.

Movie 3. Simulation of fast-slow reentry using the cellular automaton model. Responses to S1 and S2 stimuli are shown. S1-S2 interval, 96 ms. The preparation was stimulated at the His bundle as shown by the stimulating electrodes. There is a flash and click coincident with each stimulus. Same data as shown in Fig. 8B,C.

Movie 4. Simulation of slow-fast reentry and the effect of slow pathway ablation. Cellular automaton model used. Responses to S1 and S2 stimuli are shown. S1-S2 interval, 96 ms. The preparation was stimulated at the crista terminalis as shown by the stimulating electrodes. There is a flash and click coincident with each stimulus. Left, slow-fast reentry under control conditions. Same data as shown in Fig. S10. Right, abolition of reentry by slow pathway ablation. The ablation site is shown. In each panel, the timing of the stimuli is shown at the top left and the timing of action potentials at the recording electrodes on the His bundle is shown at the bottom right.

Model Array Data.txt. The 3D anatomical model of the AVN. The model is an array consisting of ~13 million nodes. The model is saved as a 250 MB text file (Model Array Data.txt). The text file has been converted to an 8 MB Microsoft cabinet file (Model Array Data.cab). To view the text file, we recommend using Microsoft WordPad. The text file lists the x, y and z coordinates and the cell type of each node. 1, fat; 2, connective tissue; 3, ventricular muscle; 4, atrial muscle; 5, aortic valve; 6, transitional tissue; 7, tendon of Todaro; 8, inferior nodal extension; 9, penetrating bundle; 10, vein; 11, compact node.

Table S1. Coupling parameters used with the anatomical model of the AVN. L and T refer to the longitudinal and two transverse axes of a myocyte. g_j, coupling conductance.

	Atrial muscle (peach)	**Transitional tissue**	**Inferior nodal extension (red)**	**Penetrating bundle (purple)**
Cellular automaton model				
R_L	630 μm	630 μm	90 μm	360 μm
R_T	210 μm	210 μm	30 μm	120 μm
Monodomain model				
D_L (equivalent g_j)	1.25 cm^2/s (625 nS)	0.4 cm^2/s (160 nS)	0.1 cm^2/s (29 nS)	0.4 cm^2/s (160 nS)
D_T (equivalent g_j)	0.417 cm^2/s (208 nS)	0.133 cm^2/s (53.3 nS)	0.033 cm^2/s (9.67 nS)	0.133 cm^2/s (53.3 nS)

Table S2. Refractory periods at the rabbit AVN.

Source	**Atrial muscle**	**Fast pathway**	**Slow pathway**
J. Billette (unpublished data)	81±5 ms	127±9 ms	91±12 ms
Reid et al.[17]	-	141±15 ms	91±10 ms
Lin et al.[18]	-	-	100±9 ms

Table S3. Refractory periods (E_i+P_i) used in the cellular automaton model.

Atrial muscle (peach)	**Transitional tissue (green)**	**Inferior nodal extension (red)**	**Penetrating bundle (purple)**
81 ms	134 ms	94 ms	94 ms

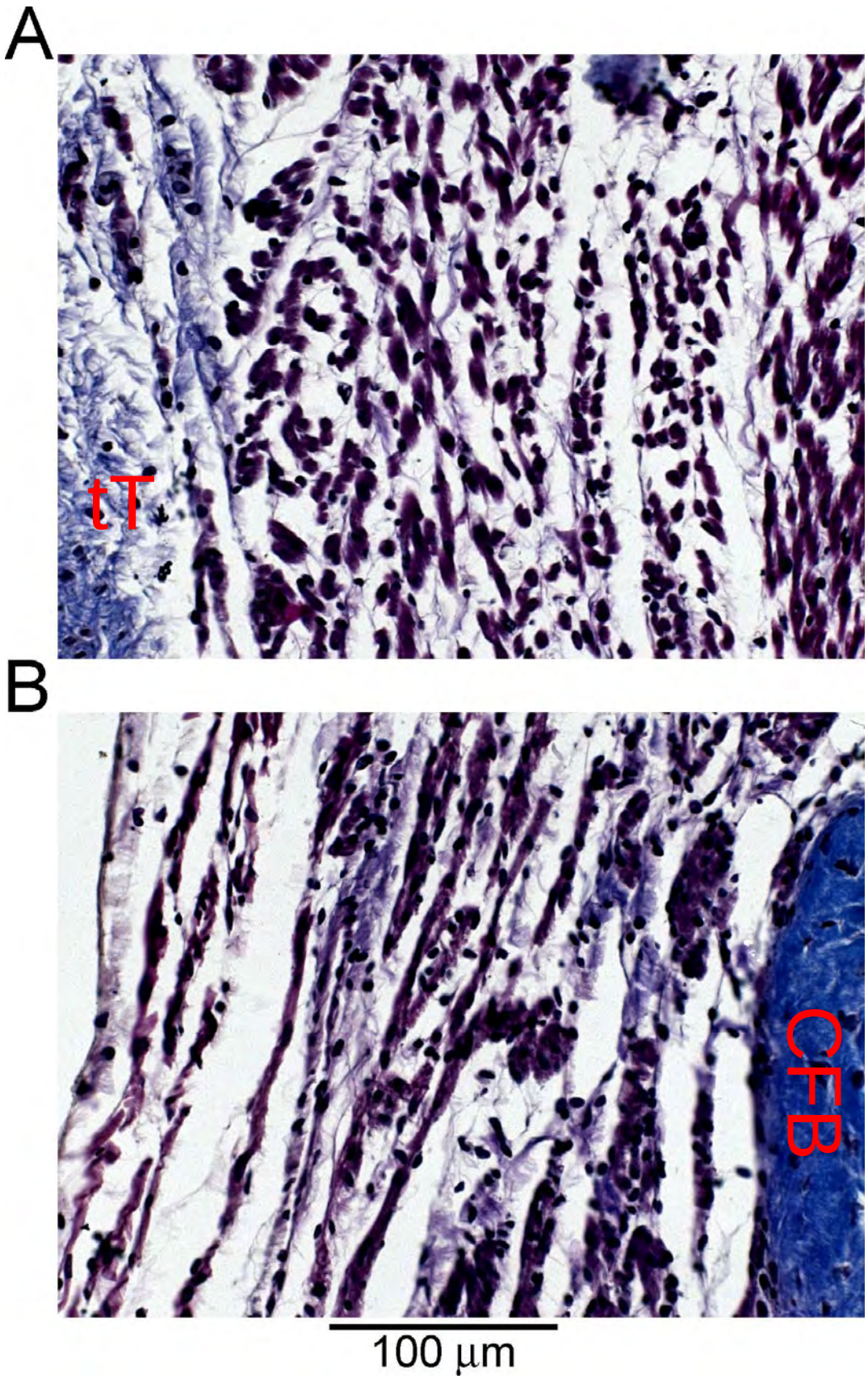

Figure S1. Measurement of myocyte orientation. Two high magnification images of the Masson's trichrome stained section corresponding to the boxed regions in Fig. 6A are shown. A shows transitional tissue next to the tendon of Todaro (blue; tT). The majority of the myocytes (purple) appear to be sectioned transversely (resulting in a circular cross-section) and the myocytes are assumed to be running perpendicular to the section. B shows (from left to right) transitional tissue, nodal tissue and the central fibrous body (blue; CFB). The majority of myocytes appear to be sectioned longitudinally (resulting in a long elliptical cross-section) and the myocytes are assumed to be running in the plane of the section (at an angle of ~45°).

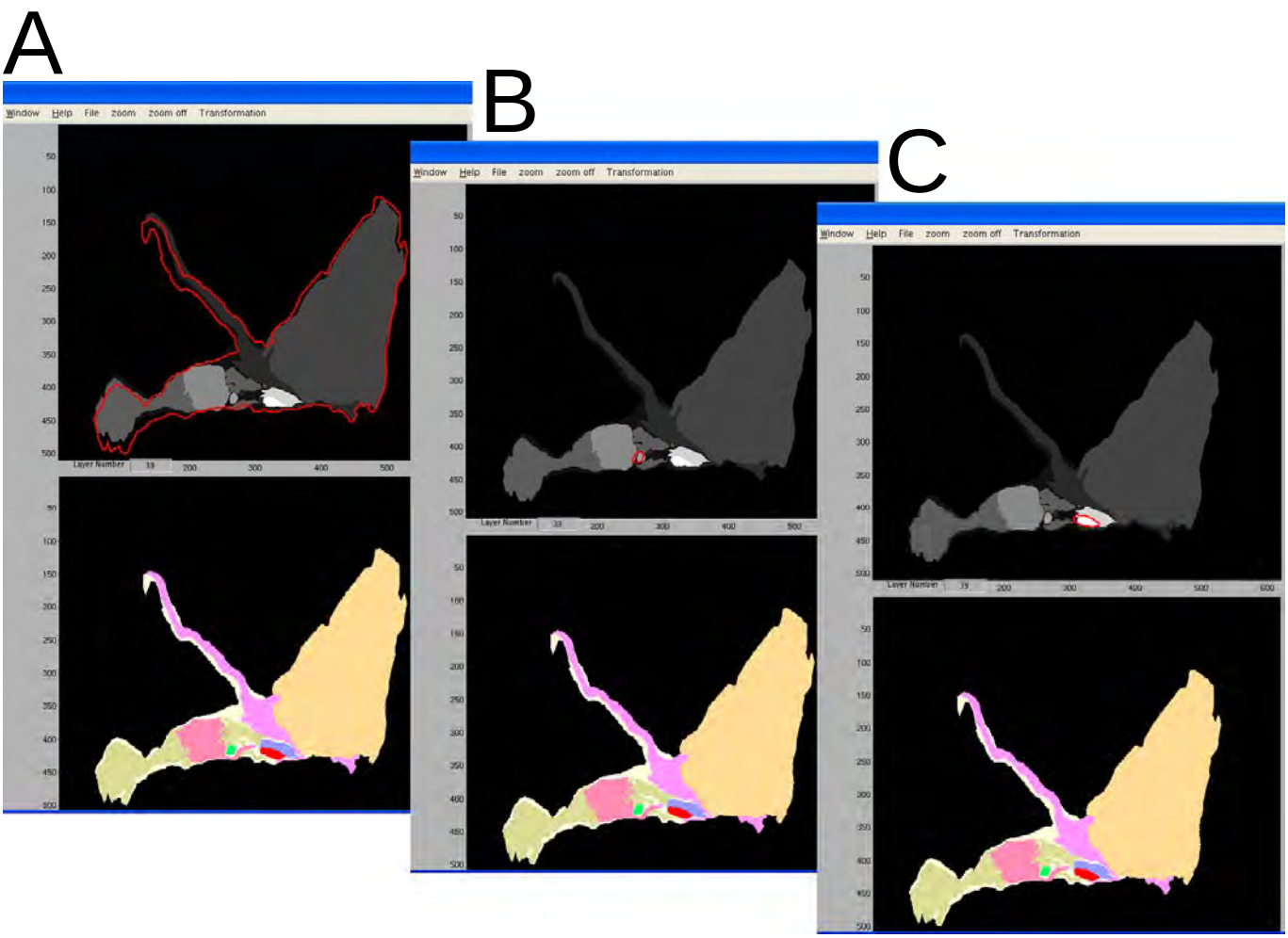

Figure S2. Three screenshots from the custom written programme used for correction and alignment. The current model section being worked on is shown in colour in the bottom half of the screen; the previous section is shown in greyscale in the top half of the screen. A, outline of the current section (shown in red in the top half of the screen). B, outline of the tendon of Todaro in the current section (shown in red in the top half of the screen). C, outline of the compact node in the current section (shown in red in the top half of the screen).

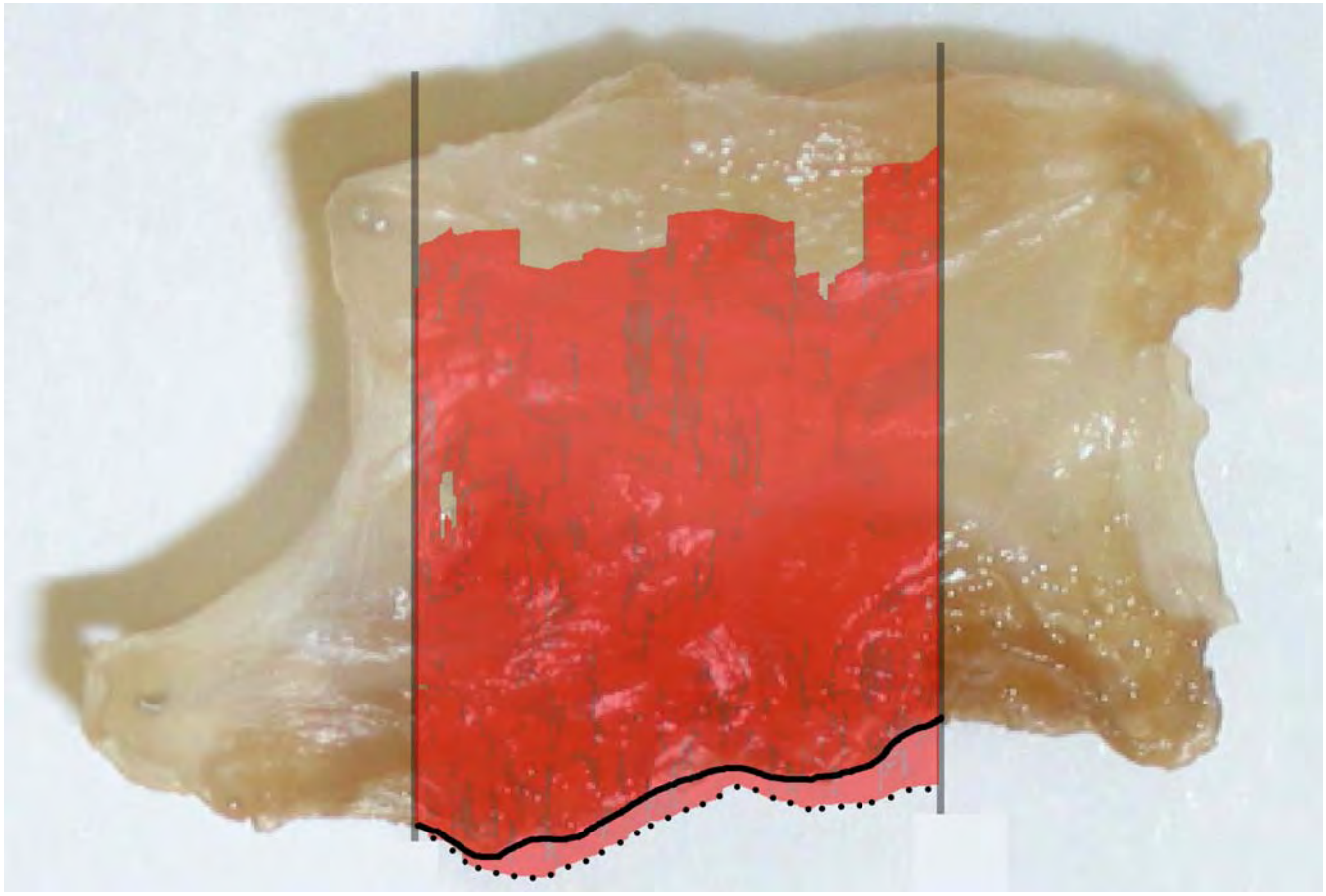

Figure S3. Envelope of the model sections superimposed on a photograph of the original preparation. Dotted line, bottom edge of the original envelope of model sections. Solid line, bottom edge of the original preparation.

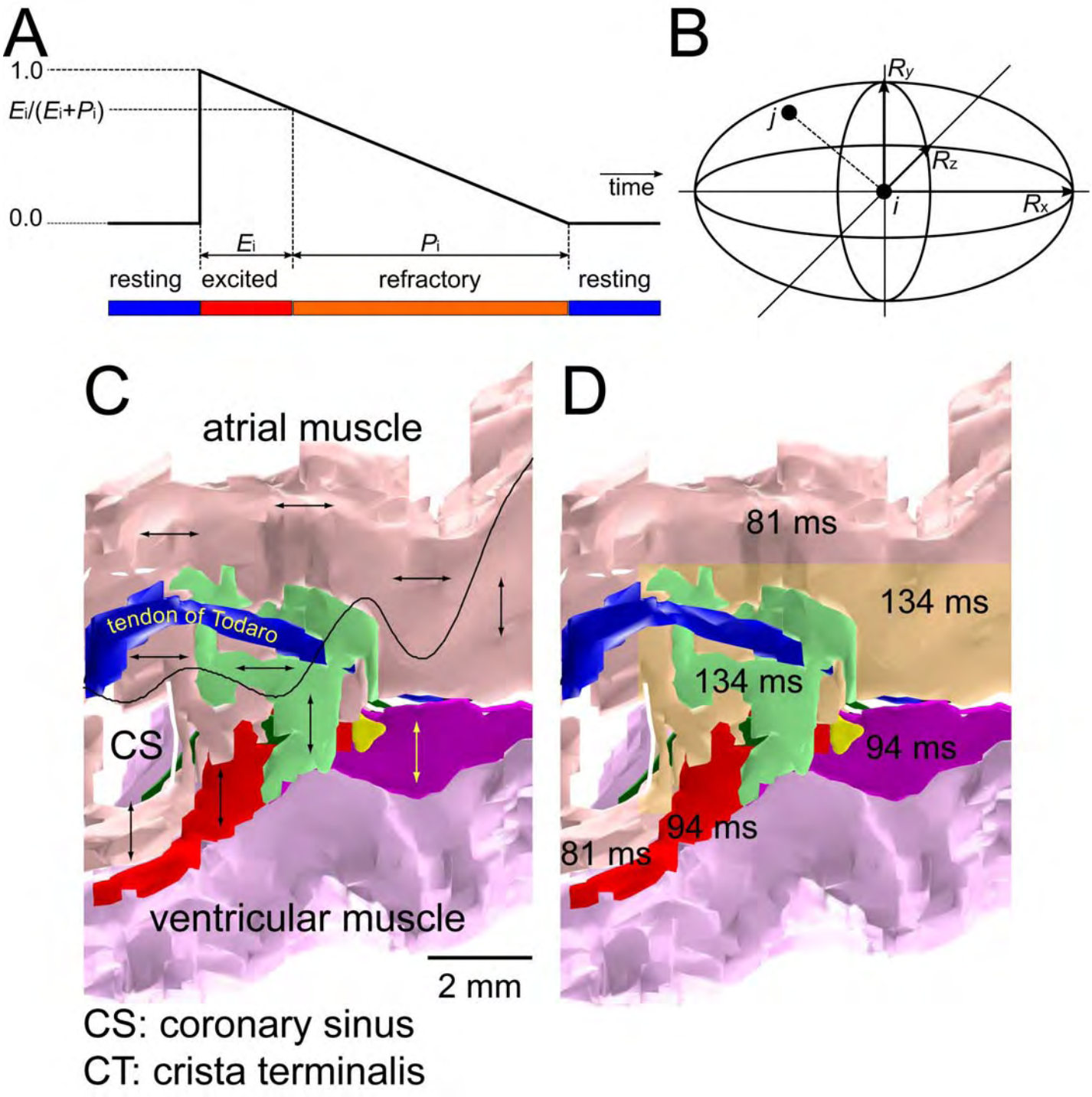

Figure S4. Cellular automaton model. A, time course of state (u) of node i. If the node is excited, the node state is changed from 0 (resting) to 1 (excited). The node state then declines back to 0. B, definition of neighbouring nodes of node i. If node j is an ellipsoid centred on node i, node j is defined as a neighbouring node of node i. The parameters, R_x, R_y and R_z, determine the shape of the ellipsoid and, therefore, account for the anisotropy of cardiac tissue (the dependence of conduction velocity on cell orientation) and coupling conductance. C, D, myocyte orientation (C) and refractory periods (D) in the anatomical model of the AVN used in the simulation of action potential conduction. In C, the arrows show myocyte orientation.

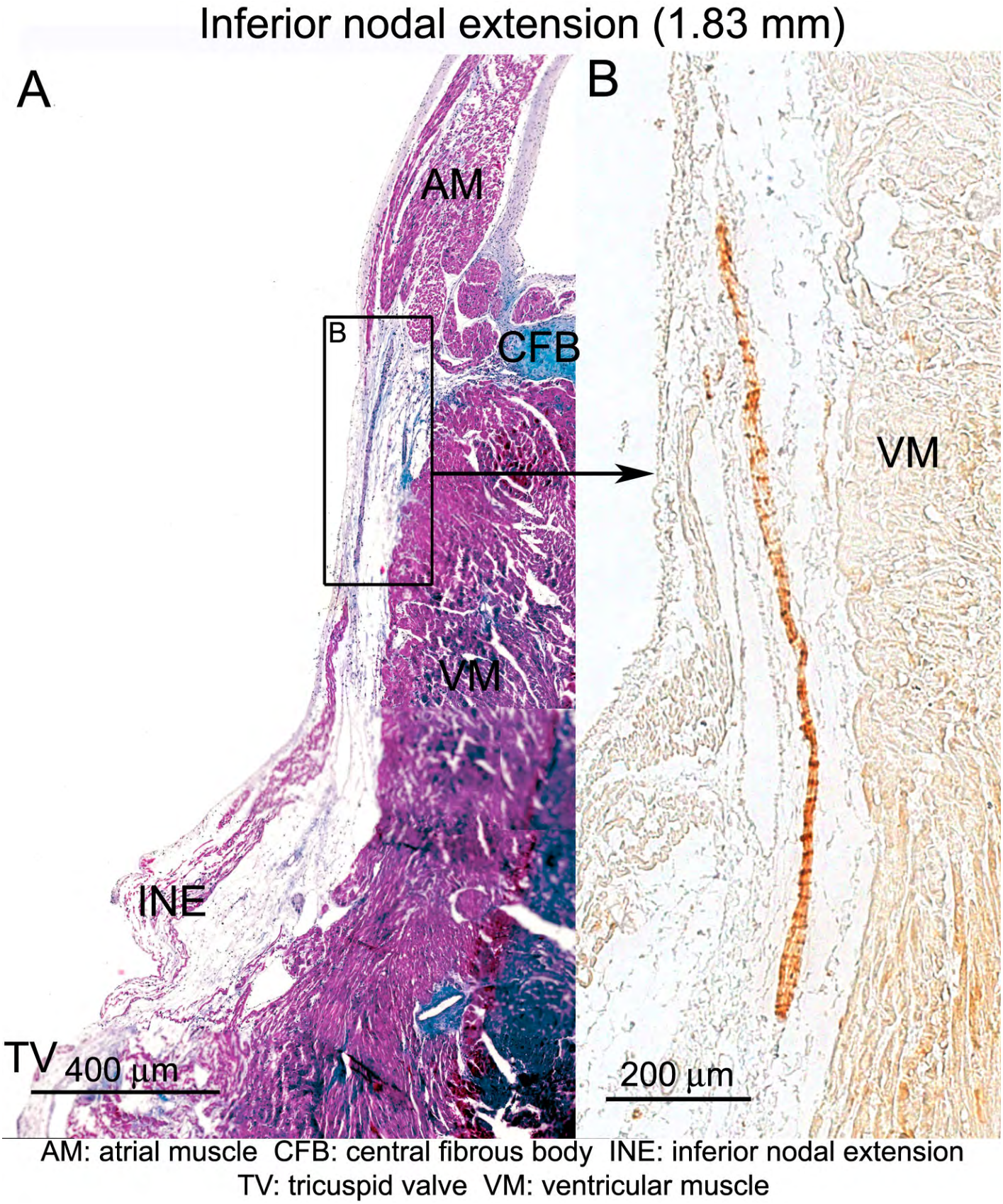

Figure S5. Nerve trunk at the inferior nodal extension. A, Masson's trichrome stained section. B, adjacent neurofilament labelled section. From box B in A.

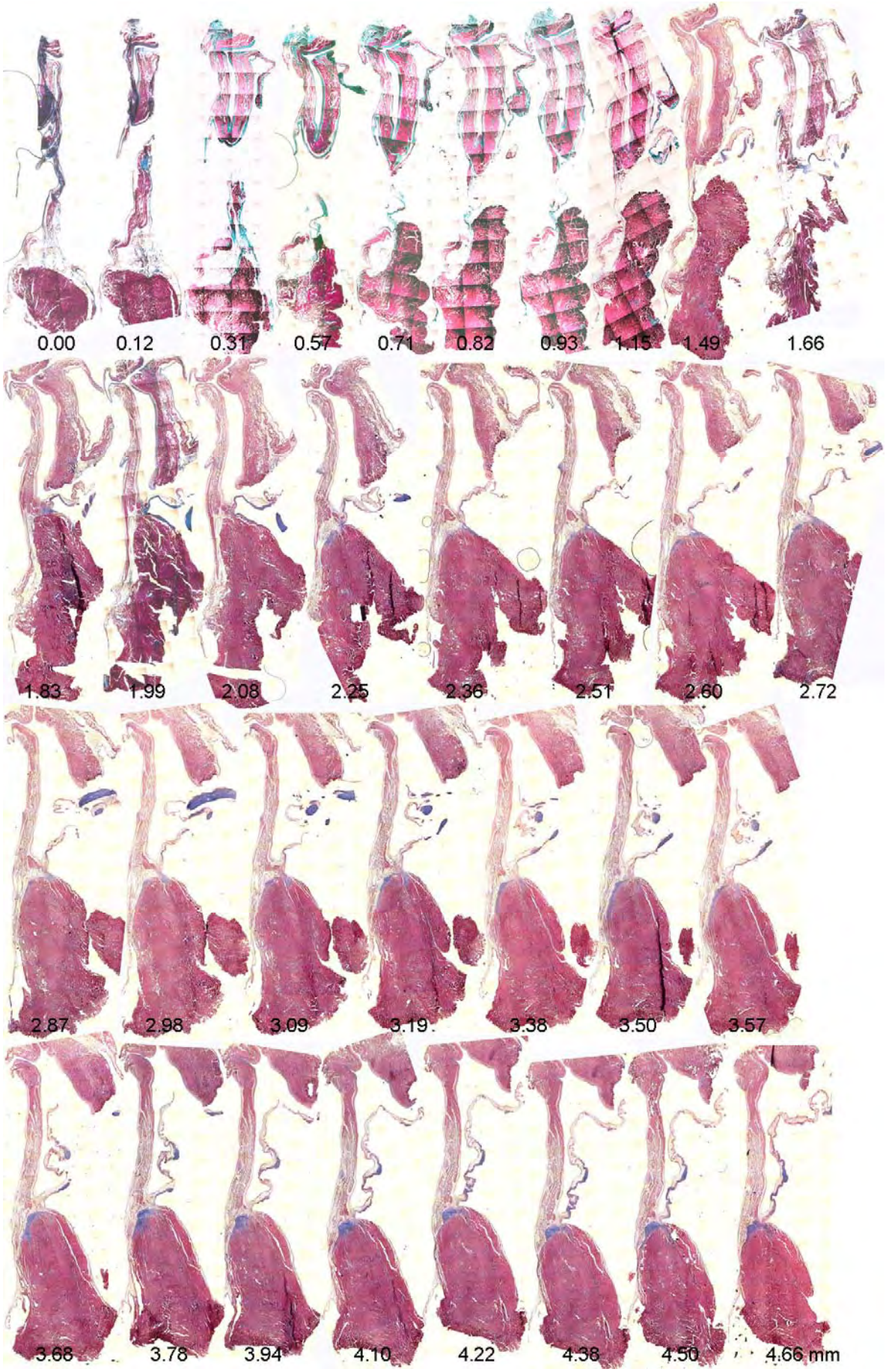

Figure S6. Masson-trichrome stained sections at the 65 levels on which the 3D anatomical model is based – part 1. Distances in mm shown (see Fig. 1B). Note the densely-packed bundle of atrial muscle on the right hand side of the preparation immediately above the central fibrous body extending from 2.36 to 4.66 mm (at least).

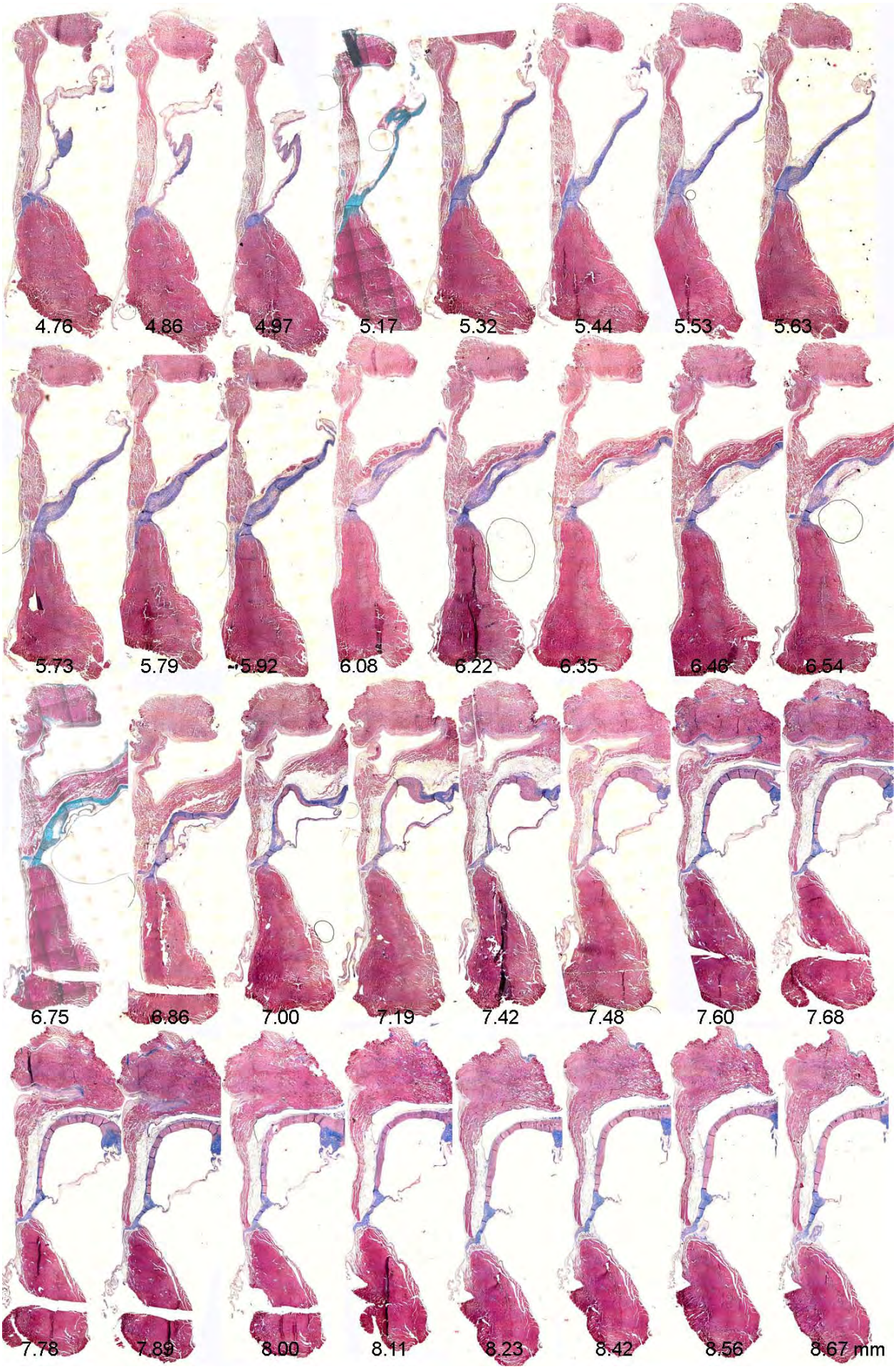

Figure S7. Masson-trichrome stained sections at the 65 levels on which the 3D anatomical model is based – part 2. Distances in mm shown (see Fig. 1B).

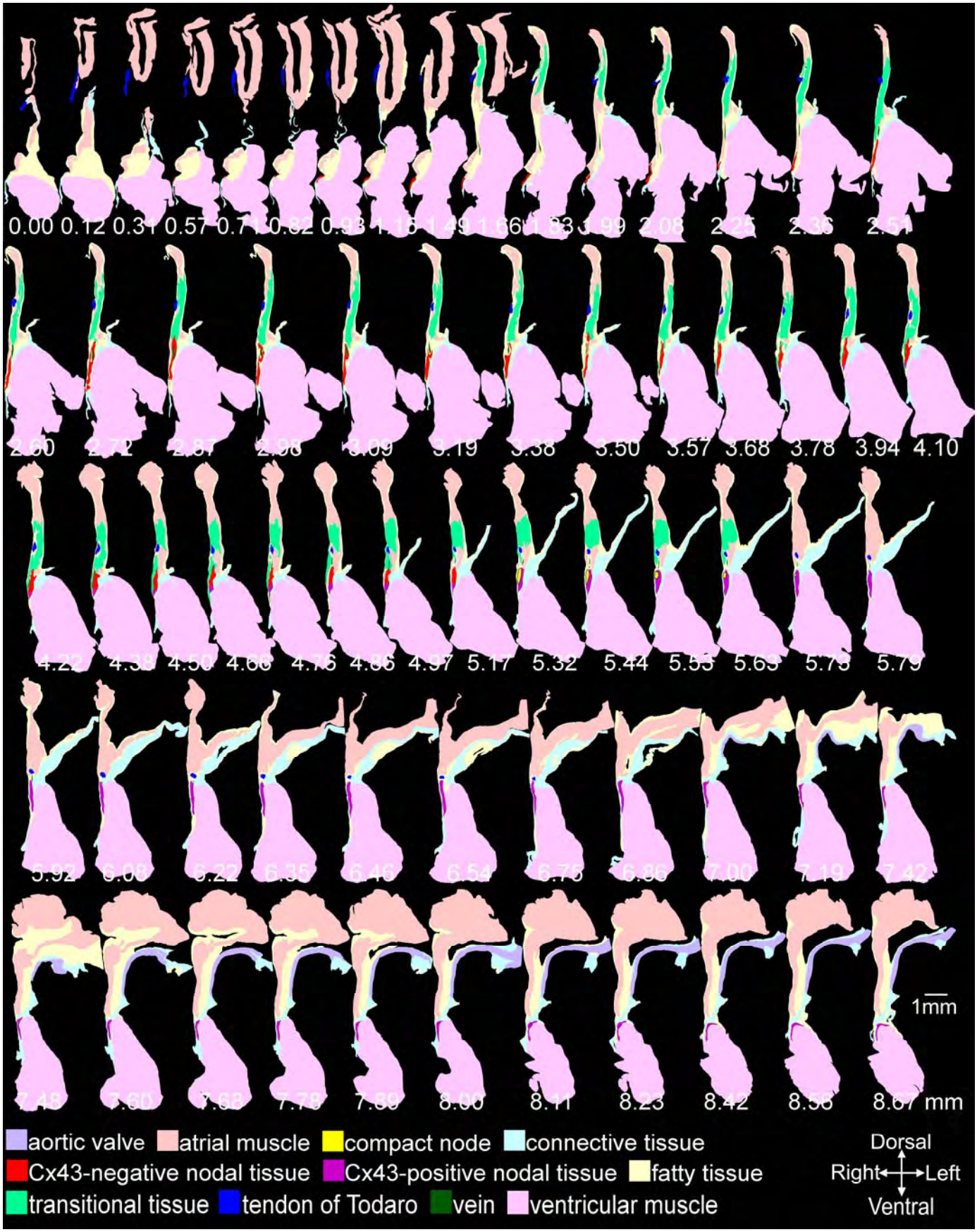

Figure S8. 65 model sections used to construct the 3D anatomical model of the AVN. The whole of the sections are shown. Distances in mm shown (see Fig. 1B).

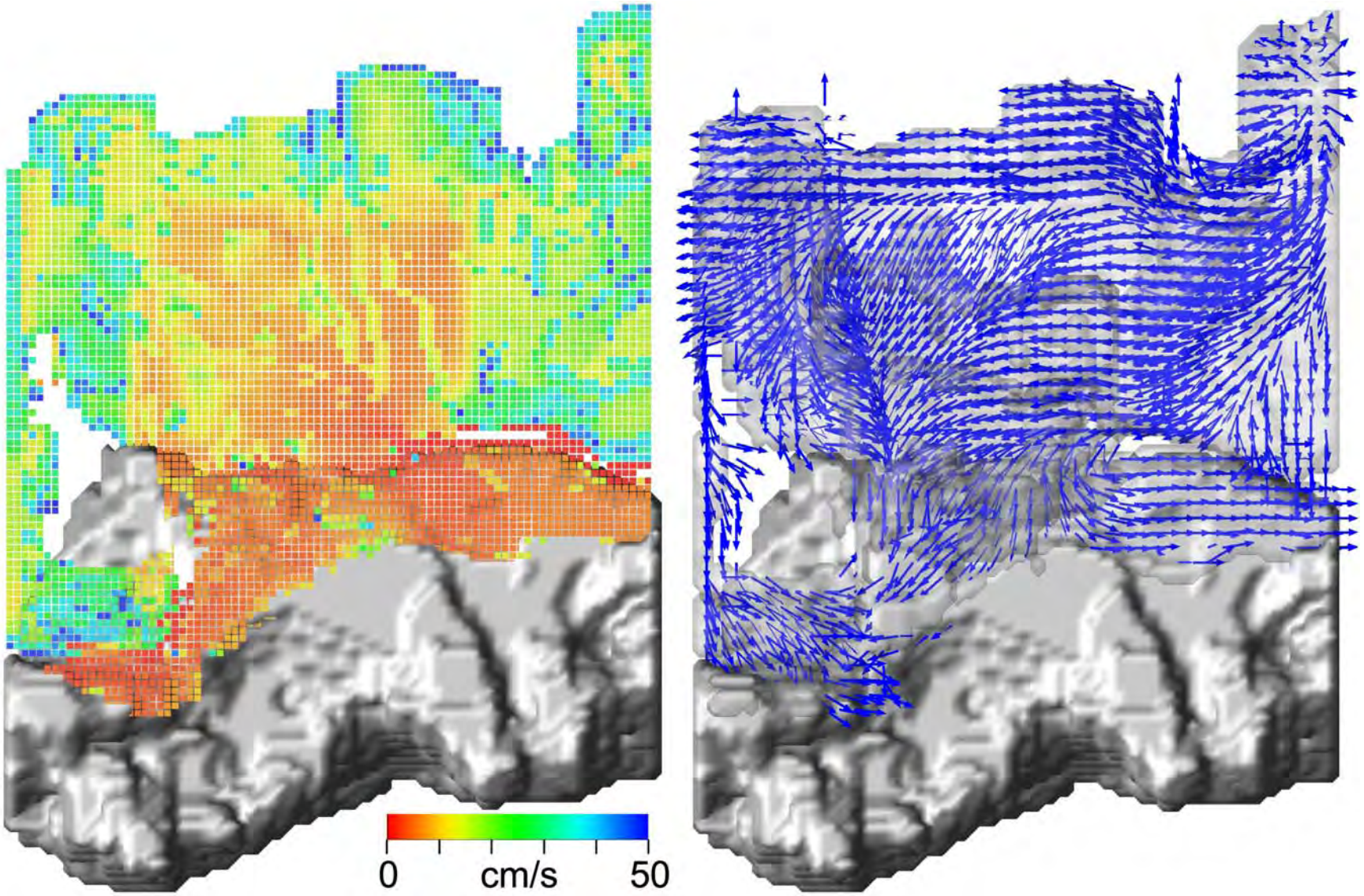

Figure S9. Local conduction velocities. Left, magnitude of local conduction velocity. Right, direction of local conduction (shown as arrows). The data are calculated from the simulation shown in Fig. 8A.

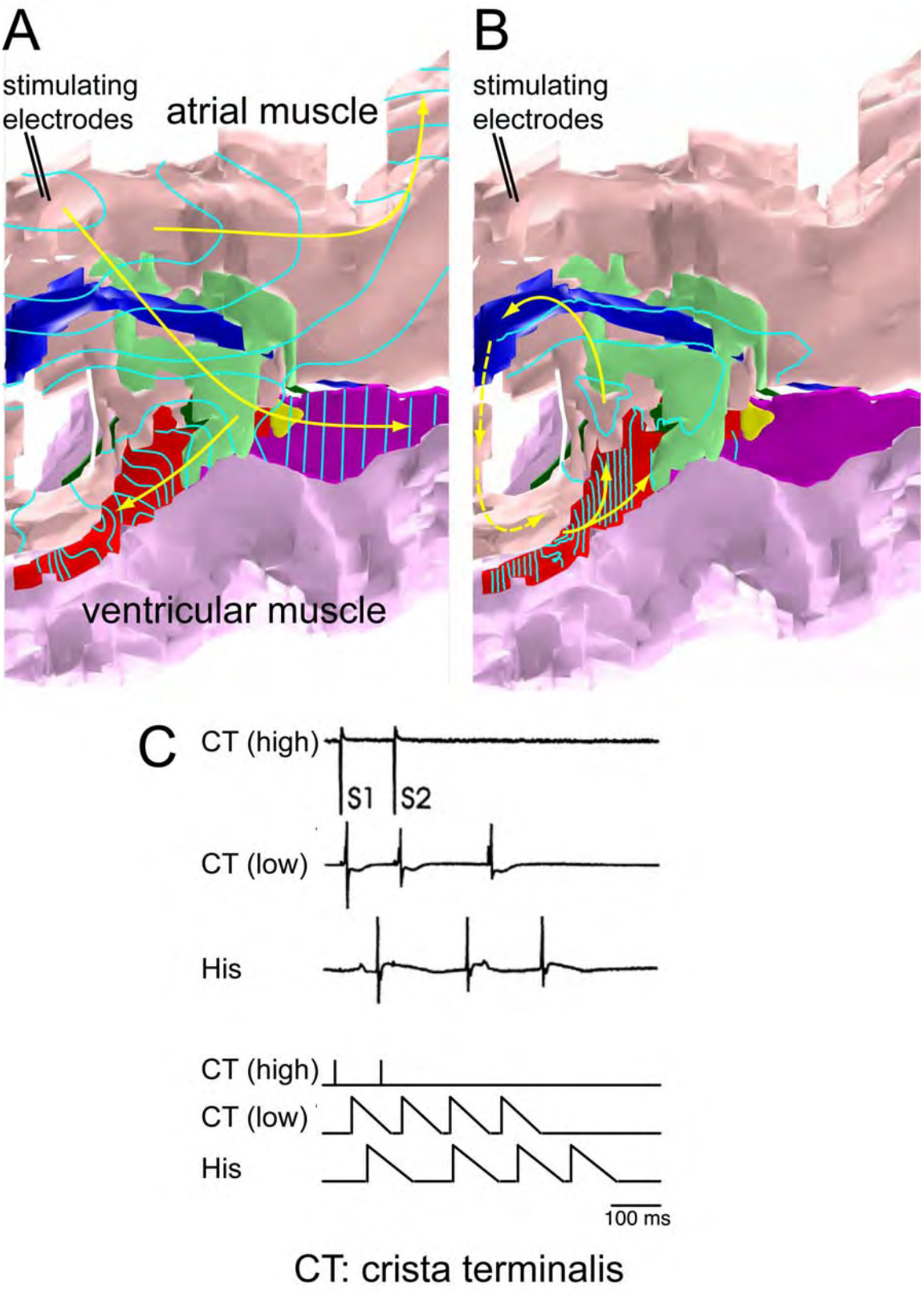

Figure S10. Simulation of slow-fast reentry using the cellular automaton model. A, B, simulation of the activation sequence during slow-fast reentry at the AVN. The preparation was stimulated using a S1-S2 protocol (S1-S2 interval, 96 ms). The isochrones (at 5 ms intervals) and yellow arrows show the propagation of the action potential: A shows the propagation of the S1 action potential and B shows the propagation of the S2 action potential. C, extracellular potentials recorded at the crista terminalis (at high and low sites) and His bundle of the rabbit AVN conduction axis during slow-fast reentry (top; S1-S2 interval, 110 ms; from Nikolski et al.[1]) and equivalent signals from equivalent sites in the simulation of slow-fast reentry (bottom; from the simulation shown in A and B). In both experiment and simulation, the crista terminalis (high) was the stimulation site.